RESEARCH ARTICLE | OCTOBER 15 2024

Cavity Born–Oppenheimer approximation for molecules and materials via electric field response

Special Collection: Polaritonics for Next Generation Materials

John Bonini ; Iman Ahmadabadi ; Johannes Flick

J. Chem. Phys. 161, 154104 (2024)
https://doi.org/10.1063/5.0230983
CHORUS

The Journal of Chemical Physics ARTICLE pubs.aip.org/aip/jcp

Cavity Born–Oppenheimer approximation for molecules and materials via electric field response

Cite as: J. Chem. Phys. 161, 154104 (2024); doi: 10.1063/5.0230983
Submitted: 27 July 2024 • Accepted: 29 September 2024 •
Published Online: 15 October 2024

John Bonini,[1,2,a)] Iman Ahmadabadi,[2,3,4] and Johannes Flick[2,5,6,b)]

AFFILIATIONS

[1] Material Measurement Laboratory, National Institute of Standards and Technology, 100 Bureau Dr., Gaithersburg, Maryland 20899, USA
[2] Center for Computational Quantum Physics, Flatiron Institute, 162 5th Avenue, New York, New York 10010, USA
[3] Joint Quantum Institute, NIST and University of Maryland, College Park, Maryland 20742, USA
[4] Department of Chemistry, Princeton University, Princeton, New Jersey 08544, USA
[5] Department of Physics, The City College of New York, 160 Convent Ave., New York, New York 10031, USA
[6] Department of Physics, The Graduate Center, City University of New York, New York, New York 10016, USA

Note: This paper is part of the JCP Special Topic on Polaritonics for Next Generation Materials.
[a)] **Electronic mail:** john.bonini@nist.gov
[b)] **Author to whom correspondence should be addressed:** jflick@ccny.cuny.edu

ABSTRACT

We present an *ab initio* method for computing vibro-polariton and phonon-polariton spectra of molecules and solids coupled to the photon modes of optical cavities. We demonstrate that if interactions of cavity photon modes with both nuclear and electronic degrees of freedom are treated on the level of the cavity Born–Oppenheimer approximation, spectra can be expressed in terms of the matter response to electric fields and nuclear displacements, which are readily available in standard density functional perturbation theory implementations. In this framework, results over a range of cavity parameters can be obtained without the need for additional electronic structure calculations, enabling efficient calculations on a wide range of parameters. Furthermore, this approach enables results to be more readily interpreted in terms of the more familiar cavity-independent molecular electric field response properties, such as polarizability and Born effective charges, which enter into the vibro-polariton calculation. Using corresponding electric field response properties of bulk insulating systems, we are also able to obtain the Γ point phonon-polariton spectra of two dimensional (2D) insulators. Results for a selection of cavity-coupled molecular and 2D crystal systems are presented to demonstrate the method.

I. INTRODUCTION

The coupling of electromagnetic field excitations of optical cavities with matter has gained recent interest as a means of manipulating material and molecular properties and processes.[1,2] The modification of these excitations via optical cavities has been reported experimentally for various characteristics, such as chemical reactivity,[3] optical spectra,[4,5] relaxation dynamics and ultrafast thermal modification,[6] intermolecular vibrational energy redistribution,[7] enhancement of ferromagnetism,[8] and thermal control of metal-to-insulator transition.[9]

At the same time, these experimental developments have sparked theoretical developments of first-principles methods.[10–13] In the vibrational strong coupling (VSC) regime, where a photonic (cavity) mode becomes resonant with a vibrational/phonon mode, creating vibro-polaritonic states, the so-called cavity Born–Oppenheimer approximation (CBOA)[14,15] has been applied successfully. The CBOA approach treats low-frequency cavity modes, such as infrared modes, and nuclei as relatively slow-moving components, in comparison with the fast-moving electrons.[15] Thus, CBOA treats photons and nuclei equally, allowing for the calculation of adiabatic potential energy surfaces (PESs). For the vibrational

strong coupling regime, the CBOA has been applied to describe the chemical reactivity[16–18] and the spectra of vibro-polariton states,[19] among others.[20–24]

In this article, we present a methodology for obtaining the modification of vibrational modes in molecular systems and insulating 2D solids by coupling matter to low-frequency photon modes in optical cavities. Results of this method are shown to be equivalent to the linear response framework based on the CBOA[19] but use only the first-order electronic response to electric field and nuclei displacement perturbations as an input. Using a mapping of the CBOA energy functional to a finite field enthalpy, we can also utilize existing standard *ab initio* finite electric field response methods based on the modern theory of polarization[25,26] to calculate the cavity modified phonon spectra in solids. We show that this formalism can be generalized to multiple photon modes. Therefore, this mapping allows us to have a clear understanding of the relation between PES inside and outside the cavity. In addition, this method yields an improvement in computational efficiency of the techniques previously developed[19] for the linear response theory of vibro-polaritons in insulating materials. We present several examples for modulation of phonons in hexagonal boron nitride (h-BN), HfS_2 as a transition metal dichalcogenide (TMD), and CO_2 and $Fe(CO)_5$ as two molecular examples to demonstrate the method.

II. FORMALISM

A. Review of mean field CBOA

Within the dipole approximation, light is assumed to couple to matter through the dipole moment μ of the matter system, which has both nuclear and electronic contributions, i.e., $\mu = \mu_e + \sum_I Z_I R_I$. This is a reasonable assumption for charge-neutral, nonmagnetic systems coupled to photon fields that are approximately spatially uniform across the matter charge distribution. The minimal coupling Hamiltonian within the length gauge and dipole approximation is given by $\hat{H} = \hat{T}_e + \hat{T}_{\text{nuc}} + \hat{T}_{\text{pht}} + \hat{V}_{\text{Coulomb}} + \hat{V}_{\text{dipole}}$ with[14,19]

$$\hat{V}_{\text{dipole}} = \frac{1}{2}\sum_\alpha (\omega_\alpha \hat{q}_\alpha - \boldsymbol{\lambda}_\alpha \cdot \hat{\mu})^2, \tag{1}$$

where $\hat{q}_\alpha$ corresponds to the local displacement field of photon mode α with parameters ω_α and λ_α characterizing the photon mode of the empty cavity (which is in general dependent on the mirrors and geometry) with ω_α representing the photon mode frequency, λ_α being a vector with direction indicating the mode photon mode polarization, and magnitude indicating the amplitude of photon field oscillations at the matter position.[27]

In the CBOA,[14,15,19] q_α are treated as "slow variables" along with nuclei coordinates R_I. An effective potential for these slow variables is then constructed from the ground state energies of the electronic Hamiltonian $\hat{H}_e(R,q) = \hat{T}_e + \hat{V}_{\text{Coulomb}}(R) + \hat{V}_{\text{dipole}}(R,q)$ solved at static coordinates (R,q) yielding the system of equations,

$$\hat{H}_e(R,q)|\psi(R,q)\rangle = U(R,q)|\psi(R,q)\rangle, \tag{2}$$

$$(\hat{T}_{\text{nuc}} + \hat{T}_{\text{pht}} + \tilde{U}(R,q))|\Phi^{\text{nuc,pht}}\rangle = E|\Phi^{\text{nuc,pht}}\rangle, \tag{3}$$

where $\tilde{U}(R,q)$ corresponds to the solution of Eq. (2) with the lowest energy $U(R,q)$ occurring at an electronic ground state $\bar{\psi}_U(R,q)$.[28]

In what follows, we will treat the electronic dipole squared term [dipole-self energy (DSE)] in V_{dipole} [Eq. (1)] with a mean-field approximation, where only leading order terms in $\lambda_\alpha \cdot \hat{\mu} - \langle \lambda_\alpha \cdot \hat{\mu} \rangle$ are retained; the dipole squared term may be approximated as

$$(\lambda_\alpha \cdot \hat{\mu})^2 \overset{\text{MF}}{\approx} 2(\lambda_\alpha \cdot \langle \hat{\mu} \rangle)(\lambda_\alpha \cdot \hat{\mu}) - (\lambda_\alpha \cdot \langle \hat{\mu} \rangle)^2, \tag{4}$$

where $\langle \cdots \rangle$ is the expectation value evaluated for the electronic state at fixed (R,q). To make the function dependence more explicit, a dipole expectation value $\langle \hat{\mu} \rangle$ will be written as a function in terms of the nuclei coordinate and electronic state as $\mu(\psi,R)$. Then, $\tilde{U}(R,q)$ is found via a self-consistent solution to Eq. (2), where H_e is replaced with

$$\begin{aligned}\hat{H}_e^{\text{MF}}(\psi;R,q) = \hat{T}_e + \hat{V}_{\text{Coulomb}}(R) + \sum_\alpha \frac{1}{2}(\omega_\alpha q_\alpha)^2 \\ - (\omega_\alpha q_\alpha - \lambda_\alpha \cdot \mu(\psi,R))(\lambda_\alpha \cdot \hat{\mu}) \\ - \frac{1}{2}(\lambda_\alpha \cdot \mu(\psi,R))^2.\end{aligned} \tag{5}$$

This equation must be solved self-consistently so that ψ used to construct the Hamiltonian is equal to the resulting ground state $\bar{\psi}_U$. Self-consistent electronic solutions can be found by extending existing Kohn–Sham density functional theory (DFT) to incorporate these terms arising from $\hat{V}_{\text{dipole}}$ with existing functionals.[15,19,29]

We can consider a standard Kohn–Sham DFT functional ϵ, which takes some electronic variables ψ[30] along with nuclei coordinates R and yields some energy, which is taken as an approximation of the expectation value of the first two terms in Eq. (5),

$$\epsilon(\psi;R) \approx \langle \hat{T}_e + \hat{V}_{\text{Coulomb}}(R) \rangle_\psi, \tag{6}$$

which is minimized for fixed R at $\bar{\psi}$ so that one can consider a ground state energy as a function of R,

$$\bar{\epsilon}(R) = \epsilon(\bar{\psi};R) = \min_\psi \epsilon(\psi;R). \tag{7}$$

Then, the inclusion of $\hat{V}_{\text{dipole}}$ terms at a mean-field level corresponds to working with a new functional,

$$U(\psi;R,q) = \epsilon(\psi;R) + \frac{1}{2}\sum_\alpha (\omega_\alpha q_\alpha - \lambda_\alpha \cdot \mu(\psi,R))^2, \tag{8}$$

which is minimized for fixed R,q at $\bar{\psi}_U$ so that one can consider a ground state energy as a function of R,q,

$$\tilde{U}(R,q) = U(\bar{\psi}_U;R,q) = \min_\psi U(\psi;R,q). \tag{9}$$

The mean field CBOA approach reviewed in this section makes use of several approximations. The dipole approximation neglects spatial changes in the photon mode amplitude across the matter and should be valid for larger photon wavelengths with appropriate cavity matter geometries. The CBOA relies on electronic excitations being higher energy than both nuclei displacements (e.g., vibrations) and the relevant photon modes and should be valid for systems with an electronic gap (e.g., molecules/insulators) in cavities where the relevant photon modes have frequencies much smaller than the gap. The self-consistent mean field approach for both the dipole

squared term and the usual energy (ϵ) via standard DFT functionals is expected to be reasonable for systems not known to exhibit a strongly correlated behavior.

B. Effective electric fields

In this work, we develop an alternative, but equivalent procedure where cavity properties can be obtained using DFT calculations with only finite electric field terms. For a given ψ, Eq. (5) has only one electronic operator from V_{dipole} and it is linear in $\hat{\mu}$. This is much like a system in a static and uniform electric field. At a self-consistent solution $\tilde{\psi}_U$, it is as if there is an effective electric field coupling linearly with the dipole operator given by $\mathbb{E} = \sum_\alpha \lambda_\alpha \mathcal{E}_\alpha$, where

$$\mathcal{E}_\alpha = \omega_\alpha q_\alpha - \lambda_\alpha \cdot \tilde{\mu}_U(R,q) \tag{10}$$

and $\tilde{\mu}_U(R,q) = \mu(\tilde{\psi}_U; R, q)$. Since $\tilde{\psi}_U$ is a fixed point in a procedure for finding self-consistent solutions to Eq. (5), the terms corresponding to expectation values act as constants. So long as there is not a lower energy state for the same effective electric field (e.g., as can occur in ferroelectric materials in regions where $\partial^2 \tilde{U}/\partial q^2 < 0$), then the resulting electronic ground state $\tilde{\psi}_U$ will also be a fixed point of a procedure self-consistently minimizing the enthalpy functional,

$$\mathcal{F}(\psi; R, \mathcal{E}) = \epsilon(\psi; R) - \mathbb{E}(\mathcal{E}) \cdot \mu(\psi, R_I). \tag{11}$$

This functional is minimized for fixed R, $\mathcal{E}$ at $\tilde{\psi}_\mathcal{F}$ so that one can consider a ground state enthalpy as a function of R, $\mathcal{E}$,

$$\tilde{\mathcal{F}}(R, \mathcal{E}) = \mathcal{F}(\tilde{\psi}_\mathcal{F}; R, q) = \min_\psi \mathcal{F}(\psi; R, \mathcal{E}). \tag{12}$$

Self-consistent minimization of this functional is already implemented in many DFT codes either as a linear external potential or via a Berry phase formalism to treat insulating systems with periodic boundary conditions.[26]

The relation between Eqs. (8) and (12) is quite similar to the relation between the static displacement field and static electric field functionals identified in Ref. 31, which was presented in the context of bulk dielectrics. Analogously to that work, we can derive the relation between Eqs. (8) and (11) in terms of the Legendre transform (LT) of Eq. (8). We start by defining $\mathcal{E}_\alpha$ to be the conjugate variable to the quantity $\mathcal{D}_\alpha := \omega_\alpha q_\alpha$. Then, so long as Eq. (8) is convex with respect to q_α, the LT of $U(\psi, R, d)$, which we label as $\mathfrak{F}(\psi, R, \mathcal{E})$, is then given by

$$\mathfrak{F} := U - \sum_\alpha \mathcal{D}_\alpha \mathcal{E}_\alpha, \tag{13}$$

where

$$\mathcal{E}_\alpha := \frac{\partial U}{\partial \mathcal{D}_\alpha}, \tag{14}$$

$$\mathcal{D}_\alpha := -\frac{\partial \mathfrak{F}}{\partial \mathcal{E}_\alpha}, \tag{15}$$

of which Eq. (14) provides a systematic means of arriving at Eq. (10). The LT of U written in terms of $\mathcal{E}_\alpha$ is then

$$\mathfrak{F}(\psi, R, \mathcal{E}) = \tilde{\epsilon}(\psi, R) - \sum_\alpha \mathcal{E}_\alpha \lambda_\alpha \cdot \tilde{\mu}_\mathcal{F}(\psi, R) - \frac{1}{2}\sum_\alpha \mathcal{E}_\alpha^2. \tag{16}$$

This function differs from $\mathcal{F}$ only by the term $-\frac{1}{2}\sum_\alpha \mathcal{E}_\alpha^2$, which is constant for fixed $\mathcal{E}$, and thus, minimizing F at fixed $\mathcal{E}$ with respect to ψ would yield the same $\tilde{\psi}_\mathcal{F}$ as defined in Eq. (12).

In terms of differentials, we have

$$dU = \frac{\partial U}{\partial \psi} d\psi + \frac{\partial U}{\partial R} dR + \mathcal{E} d\mathcal{D}, \tag{17}$$

and using Eq. (15),

$$d\mathfrak{F} = \frac{\partial \mathfrak{F}}{\partial \psi} d\psi + \frac{\partial \mathfrak{F}}{\partial R} dR - \mathcal{D} d\mathcal{E}. \tag{18}$$

Since $\mathfrak{F} := U - \sum_\alpha \mathcal{D}_\alpha \mathcal{E}_\alpha$, we also have

$$d\mathfrak{F} = dU - \mathcal{E} d\mathcal{D} - \mathcal{D} d\mathcal{E} \tag{19}$$

so that

$$d\mathfrak{F} = \frac{\partial U}{\partial \psi} d\psi + \frac{\partial U}{\partial R} dR - \mathcal{D} d\mathcal{E}. \tag{20}$$

Since $\frac{d\mathfrak{F}}{d\psi}|_{R\mathcal{E}} = \frac{dU}{d\psi}|_{R\mathcal{D}}$, the electronic state $\tilde{\psi}_\mathcal{F}$, which minimizes $\mathfrak{F}$ (and $\mathcal{F}$) at fixed R, $\mathcal{E}$, will also minimize U at fixed R, $\mathcal{D}$. At the electronic ground state, $\frac{\partial U}{\partial \psi} = 0$, so the force F_I on the Ith nuclei is given by

$$F_I = -\frac{d\tilde{U}}{dR_I}|_\mathcal{D} = -\frac{d\tilde{\mathcal{F}}}{dR_I}|_\mathcal{E}. \tag{21}$$

Thus, forces on nuclei computed as derivatives of $\tilde{\mathcal{F}}$ with respect to R_I are equal to those obtained from the corresponding derivatives of $\tilde{U}$. The effective force F_α on the photon mode variable q_α is

$$F_\alpha = -\frac{d\tilde{U}}{dq_\alpha}|_R = -\omega_\alpha \frac{d\tilde{U}}{d\mathcal{D}_\alpha}|_R = -\omega_\alpha \mathcal{E}_\alpha, \tag{22}$$

where Eq. (14) was used to arrive at the last equality.

It can be advantageous to compute properties of light–matter coupled systems by transforming results obtained via Eq. (11) rather than using a direct implementation of Eq. (5). Not only is Eq. (11) already integrated into many first-principles codes, but also cavity parameters such as $\lambda_\alpha, \omega_\alpha$ enter only in the transformation, implemented as a computationally cost-effective post-processing step, so that a range of such parameters can be obtained from an initial set of first-principles calculations. However, while it is simple to obtain the electric field parameters $\mathcal{E}_\alpha(R,q)$ from a known $\tilde{\mu}_U(R,q)$, this function cannot be obtained directly from electric field calculations where one instead can only access $\tilde{\mu}_\mathcal{F}(R,\mathcal{E}) = \mu(\tilde{\psi}_\mathcal{F}, R, \mathcal{E})$. It is only when $R, q, \mathcal{E}$ are such that Eq. (10) is satisfied that $\tilde{\mu}_\mathcal{F}(R,\mathcal{E}) = \tilde{\mu}_U(R,q)$.

In general, finding the electric field parameters yielding the same state as (R,q) requires solving the system of equations,

$$\mathcal{E}_\alpha(R,q) = \omega_\alpha q_\alpha - \lambda_\alpha \cdot \tilde{\mu}_\mathcal{F}\left(R, \sum_\beta \lambda_\beta \mathcal{E}_\beta(R,q)\right) \tag{23}$$

for each function $\mathcal{E}_\alpha(R,q)$. If such a relation is solved, it can then be used to obtain $\tilde{\mu}_U(R,q)$, $\tilde{U}(R,q)$, and other properties of the

light–matter coupled system by post-processing results computed for the matter at static electric fields.

Note that no additional approximations have been introduced. When a unique solution for the $\mathcal{E}_\alpha(R,q)$ functions can be found, the Kohn–Sham wavefunctions (and thus charge densities), which minimize $\mathcal{F}$ of Eq. (11) at $R, \mathcal{E}(R,q)$ also minimize $\tilde{U}$ of Eq. (8) at R, q. While no additional approximations have been made, there are some limits to when the relations can be utilized. As mentioned, the mapping only applies in regions where $\frac{\partial^2 U}{\partial q^2} > 0$. Furthermore, at large $\mathcal{E}_\alpha$, Eq. (11) may seize to have local minima as discussed in Ref. 26, although individual steps in a self-consistent procedure minimizing $\tilde{U}$ can run into the same issue. Near the ground state R, q in an insulating system, neither of these issues arise so that low order response properties can be found, provided that they can also be mapped between the $(\mathcal{E}, R) \leftrightarrow (q, R)$ change of variables.

C. Linear response framework

While in general solving Eq. (23) is non-trivial, properties such as the vibro-polariton spectra can be obtained using only linear terms in $\tilde{\mu}_{\mathcal{F}}(R,\mathcal{E})$ so that Eq. (23) becomes a linear problem. In this section, we show how vibro-polariton modes and IR spectra can be obtained from standard adiabatic response terms, namely the force constant matrix, Born effective charges, and clamped ion polarizability. Near the ground state values of R and $\mathcal{E}$ (and thus near R and q), the dipole expectation value can be expanded to linear order,

$$\tilde{\mu} = \tilde{\mu}_0 + \sum_I Z_I^* \Delta R_I + \chi \mathbb{E}, \tag{24}$$

where Z_I^* are Born effective charges $(Z_{Ii} = \frac{d\tilde{\mu}_i}{dR_I})$ and χ is the polarizability tensor $(\chi_{ij} = \frac{d\tilde{\mu}_i}{d\mathbb{E}_j})$.

Then, Eq. (23) becomes

$$\mathcal{E}_\alpha = \omega_\alpha \Delta q_\alpha - \lambda_\alpha \cdot \sum_I Z_I^* \Delta R_I - \lambda_\alpha^T \chi \sum_\beta \lambda_\beta \mathcal{E}_\beta, \tag{25}$$

where $\Delta q_\alpha = q_\alpha - \frac{\lambda_\alpha \cdot \tilde{\mu}_0}{\omega_\alpha}$. This linear system can then be solved for $\mathcal{E}_\alpha$,

$$\mathcal{E}_\alpha = \sum_\beta \left[(\mathbb{I} + \mathbb{X})^{-1}\right]_{\alpha\beta} \left(\omega_\beta \Delta q_\beta - \lambda_\beta \cdot \sum_I Z_I^* \Delta R_I\right), \tag{26}$$

where $\mathbb{I}_{\alpha\beta} = \delta_{\alpha\beta}$ is an identity matrix and $\mathbb{X}_{\alpha\beta} = \lambda_\alpha^T \chi \lambda_\beta$. Note that this λ_α dependence in $\mathbb{X}$ means that the effective field strength is not monotonic in the coupling strength. Electronic ground states found by minimizing energy via Eq. (5) at small, fixed, changes in q from the $\lambda \to 0$ ground state value are then identical to states found via fixed electric field calculations with $\mathbb{E} = \sum_\alpha \lambda_\alpha \mathcal{E}_\alpha$ using Eq. (11) with $\mathcal{E}_\alpha$ given by Eq. (26).

We next construct a second order expansion of the energy $\tilde{U}$ in both nuclei coordinates and electric field terms and then use this linear relation [Eq. (26)] to perform a change of coordinates from the $(\mathcal{E}_\alpha, R_I)$ basis to the desired (q_α, R_I) basis. Note that while we have defined the adiabatic combined light–matter energy $\tilde{U}$ as one computed self-consistently at fixed (R_I, q_α), we can nevertheless use Eq. (10) to express this energy as

$$\tilde{U}(R,\mathcal{E}) = \epsilon(\tilde{\psi}_{\mathcal{F}}; R) + \frac{1}{2}\sum_\alpha \mathcal{E}_\alpha^2. \tag{27}$$

We can obtain the (total) derivative of ϵ with respect to $\mathcal{E}_\alpha$ by applying the variation Hellmann–Feynman theorem to the $\tilde{\mathcal{F}}$ functional, which states that $d\tilde{\mathcal{F}}/d\mathcal{E}_\alpha = \partial\tilde{\mathcal{F}}/\partial\mathcal{E}_\alpha$; thus,

$$\frac{d\epsilon(\tilde{\psi}_{\mathcal{F}}; R)}{d\mathcal{E}_\alpha} = \sum_\beta \mathcal{E}_\beta \lambda_\beta \left(\chi\lambda_\alpha + \frac{d\chi}{d\mathcal{E}_\alpha}\sum_\gamma \mathcal{E}_\gamma \lambda_\gamma\right). \tag{28}$$

We focus on regimes near zero electric field and only expand energy to second order so that the second term may be dropped. At zero electric field, derivatives with nuclei are unchanged from the usual force constant matrix given by $C_{IJ} = \frac{\partial^2 \tilde{U}}{\partial R_I \partial R_J}$. Then, the energy $\tilde{U}$ to second order in $R, \mathcal{E}$ variables is given by

$$\tilde{U} = \tilde{U}(R_0, q_0) + \frac{1}{2} C_{IJ} \Delta R_I \Delta R_J + \frac{1}{2}(\delta_{\alpha\beta} + \lambda_\beta \chi \lambda_\alpha)\mathcal{E}_\alpha \mathcal{E}_\beta. \tag{29}$$

Using Eq. (26), this can be transformed to finally obtain the second order energy in the R_I, q_α coordinates,

$$\begin{aligned}\tilde{U} = \tilde{U}(R_0, q_0) &+ \frac{1}{2}\Delta R_I C_{IJ} \Delta R_J + \frac{1}{2}\left[\omega_\alpha \Delta q_\alpha - \lambda_\alpha Z_I \Delta R_I\right] \\ &\times \left[(\mathbb{I} + \mathbb{X})^{-1}\right]_{\alpha\gamma}\left[\omega_\gamma \Delta q_\gamma - \lambda_\gamma Z_J \Delta R_J\right].\end{aligned} \tag{30}$$

Equation (30) represents a key result of this work, with the CBOA energy expressed to second order in nuclei displacements ΔR_I and cavity photon displacements q_α using quantities involving only the systems' response to nuclei displacements and static electric fields.

As in Ref. 19, we can obtain IR absorption amplitudes from the normal mode eigenvectors and the derivative of the polarization with respect to each degree of freedom. Note that these quantities represent photon absorption into matter degrees of freedom through changes in the dipole moment both via displacements of nuclei and via purely electronic changes obtained using the adiabatic electronic polarizability (χ). This is not to be confused with the macroscopic absorption by the entire cavity–matter system, which includes the absorption of incident photons into confined cavity modes.

To compute the IR response amplitude, we require an expression for $\tilde{\mu}(\{q\},\{R\})$ to linear order in all q_α and R_I. Combining Eqs. (10) and (24),

$$\tilde{\mu} = \tilde{\mu}_0 + \chi\left[\sum_\alpha \boldsymbol{\lambda}_\alpha(\omega_\alpha q_\alpha - \boldsymbol{\lambda}_\alpha \cdot \mu)\right] + \sum_i \mathbf{Z}_i^* \Delta R_i \tag{31}$$

with $\tilde{\mu} = \tilde{\mu}_0 + \Delta\tilde{\mu}$,

$$\Delta\tilde{\mu} + \sum_\alpha (\chi\lambda_\alpha)\boldsymbol{\lambda}_\alpha \cdot \Delta\tilde{\mu} = \chi\sum_\alpha \boldsymbol{\lambda}_\alpha \omega_\alpha \Delta q_\alpha + \sum_i \mathbf{Z}_i^* \Delta R_i. \tag{32}$$

One can compute the 3×3 matrix $\Lambda = 1 + \sum_\alpha \chi\lambda_\alpha\lambda_\alpha^T$ (where the transpose indicates that this is an outer product), then

$$\Delta\tilde{\mu} = \Lambda^{-1}\left(\chi\sum_\alpha \boldsymbol{\lambda}_\alpha \omega_\alpha \Delta q_\alpha + \sum_i \mathbf{Z}_i^* \Delta R_i\right). \tag{33}$$

The IR amplitude for a given polariton mode is then proportional to the magnitude of $\Delta\bar{\mu}$ given by Ref. 33 using the Δq_α and ΔR_i eigendisplacements corresponding to that mode.

D. Extension to 2D periodic systems

To date, there have been only a handful of first-principles based investigations of crystal systems coupled to cavities[32–34] in part due to several challenges not faced in molecules. One challenge is that periodic systems coupled to arbitrary cavity photon modes necessitate a beyond dipole approximation treatment. Another is that working with an electronic position operator (and consequently dipole operator) requires some care in the context of periodic boundary conditions. While we do not address the former issue beyond only choosing to couple to modes that have a uniform field across the entire crystal, the formulation of the problem in terms of electronic responses to electric fields is useful in addressing the latter. Equation (30) relies only on the systems' dielectric susceptibility, Born effective charges, and force constant matrix; all these properties are routinely computed for periodic solids. Some care must be taken when adapting Eq. (30) to periodic solids as the dipole approximation is only compatible with certain cavity–matter geometries and the extrinsic quantities which enter Eq. (30) must be appropriately replaced with corresponding intrinsic quantities.

For our treatment of extended solids to be valid in the context of the dipole approximation, we require a cavity–matter geometry where the cavity photon mode profile is approximately constant over the matter (leading to a spatially uniform coupling strength). We choose a geometry of a 2D system aligned parallel and placed between two planar mirrors. Then, the confined zero momentum photon modes couple uniformly to in-plane matter dipole fluctuations. To handle periodic boundary conditions, we reformulate the problem to one in which we deal with an energy per unit cell given in terms of intrinsic properties of the system. Thus, we consider the case where the entire cavity–matter system is periodic in two dimensions with lattice vectors equal to those of the 2D unit cell of the crystal. This sort of 2D periodic cavity + matter unit cell is illustrated in Fig. 1(b). This geometry allows for a recovery of Bloch's theorem, which can be applied to both the matter and the cavity modes. Given that we are still specialized to the dipole approximation, we then treat only zero momentum (Γ point) excitations as beyond this point, the cavity portion modes have spatially modulated coupling strength over the crystal.

Then, the energy U can be considered an energy per unit cell if the dipole μ is taken to be a dipole per unit cell and the definitions of photon displacement q_α and coupling strength λ_α are also redefined for this periodic context. This can be achieved with the following substitutions for number of unit cells N: $\mu \to \mu/N$, $q_\alpha \to q_\alpha/\sqrt{N}$, and $\lambda_\alpha \to \lambda_\alpha\sqrt{N}$. One interpretation of this formulation is that the zero momentum cavity eigenstates are normalized over the periodic cavity–matter cell rather than over all space. Once these substitutions are made and the parameters of electronic susceptibility tensor χ and Born effective charge Z^* are given as derivatives of the matter dipole per unit cell rather than derivatives of the total dipole, the application of Eq. (30) is essentially unchanged; the energy is now interpreted as an energy per unit cell.

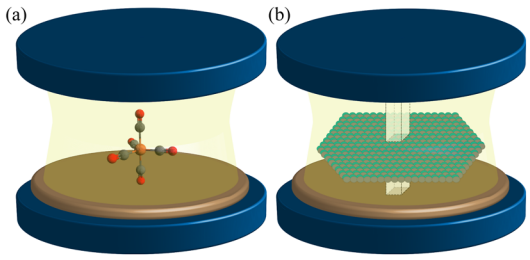

FIG. 1. Schematic illustrations of model matter + optical cavity systems. (a) A single molecule coupled to cavity photon modes. (b) A mono-layer of a 2D material arranged so that the cavity mirrors and the 2D plane of the system are parallel. The parallelepiped passing from the upper mirror through the material to the lower mirror represents the unit cell of the model used to perform calculations with periodic boundary conditions.

III. METHODS

We compute the vibro-polariton spectra for two molecules [CO_2 and $Fe(CO)_5$] and the Γ-point phonon-polariton spectra for two 2D solids (BN and HfS_2) each with various cavity parameters (ω_α and λ_α) using the formalism developed in Sec. II. For each system, we focus on cavity parameters with a cavity photon mode in resonance with the vibration mode with the largest magnitude mode effective charge (Z^*_{res}, the change in dipole with respect to vibration mode amplitude outside the cavity) where the photon mode polarization (λ_{res}) is aligned with Z^*_{res}. For each system, we compare the $|\lambda_{\text{res}}|$ dependence of Rabi splitting and matter IR absorption with and without the inclusion of the adiabatic electronic polarizability (χ) for both the cases of a single resonant cavity mode, as well as with the inclusion of additional off-resonant cavity mode harmonics. In the latter case, we choose the third relevant cavity harmonic to be in resonance with the matter system to capture the increased photon density of states at higher frequencies so that $\lambda_\alpha = \frac{\alpha}{3}\lambda_{\text{res}}$ and $\omega_\alpha = \frac{\alpha}{3}\omega_{\text{res}}$. For the two solid systems the cavity parameters are chosen to be in resonance with in plane polarized IR active phonon modes.

Matter vibrational modes, polarizabilities, and mode effective charges are computed via density functional perturbation theory (DFPT) using the Vienna *Ab initio* Simulation Package (VASP) density functional theory code[35–39] with the PBE functional[40] and an energy cutoff of 520 eV. Calculations for molecular systems were performed as Γ point only calculations in a periodic box with at least 17 Å of vacuum between periodic images along each direction. Calculations for 2D solid systems were performed on an $8 \times 8 \times 1$

TABLE I. Selected matter properties. Units for the polarizability element χ_{11} are given in Bohr radii cubed (a_0^3) for molecular systems and a_0^3 per unit cell (u.c.) for 2D crystal systems.

System	ω_{res} (meV)	χ_{11} (a_0^3)	$\lvert Z^*_{\text{res}}\rvert$ ($\frac{e}{\sqrt{\text{amu}}}$)	Degenerate
CO_2	312	26	0.75	False
$Fe(CO)_5$	252	115	0.60	False
h-BN	165	37 (u.c.)	1.10	True
HfS_2	18	316 (u.c.)	0.98	True

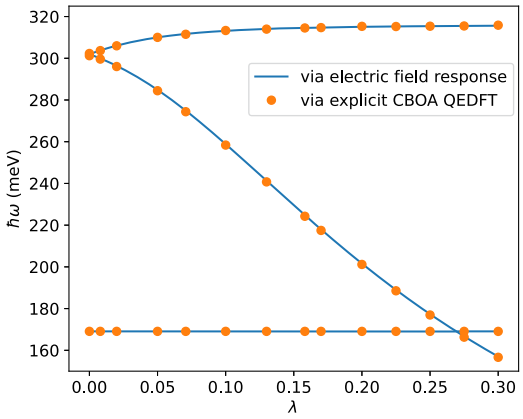

FIG. 2. Comparison of vibro-polariton splitting in CO_2 between explicit inclusion of V_{dipole} terms in Eq. (1) into the DFT energy functional[19] (orange points) and equivalent results obtained via electric field responses parameterizing the model of Eq. (30) (blue curves).

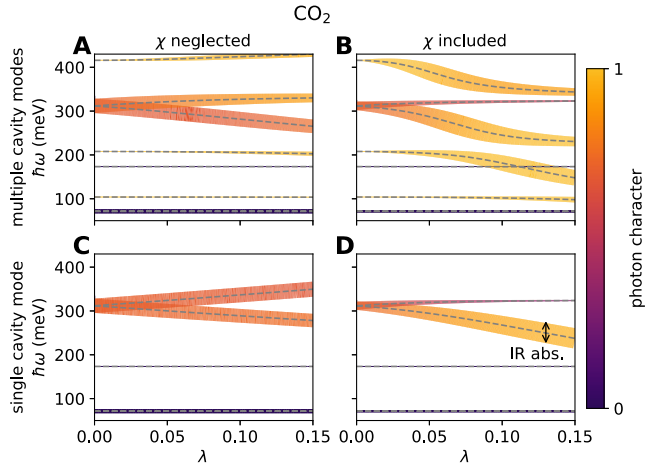

FIG. 3. Computed vibro-polariton spectrum vs coupling strength (λ) for CO_2. The thickness of curves is proportional to the IR absorption, while the color indicates the sum of the absolute values of photon components of the mode eigenvector. The right plots include the electronic polarizability term of Eqs. (30) and (33), while on the left, the value is set to zero. The spectra reveal that electronic polarizability significantly influences the strong regime of light–matter coupling, as depicted. Moreover, electronic polarizability can impact both the IR absorption and the photon components of the mode eigenvector. The lower plots indicate that calculations are performed with a single photon mode, while in the upper two plots, seven photon mode harmonics are included with the third photon mode in resonance with an IR active vibrational mode. In these upper two plots, coupling strength is scaled linearly with mode frequency and the value on the horizontal axis indicates the coupling strength of this third resonant mode.

Monkhorst-Pack grid[41] where the third dimension (orthogonal to the plane of the material) is treated as periodic with vacuum of at least 23 Å between periodic images. The most relevant matter properties are presented in Table I.

The results in Fig. 2 were obtained using the Octopus DFT code,[42] in order to provide a consistent comparison with the direct implementation of the mean field CBOA functional. There, both the effective field and direct CBOA methods used linear response performed by finite differences, as described in Ref. 19, where the results were further shown to be in agreement with the time dependent QEDFT approach of Ref. 29. Detailed computational parameters for this comparison (which are distinct from all data presented outside Fig. 2) are the same as in Ref. 19.

IV. RESULTS AND DISCUSSION

We apply the developed methodology to two molecular systems [CO_2 and $Fe(CO)_5$] and two 2D insulators (BN and HfS_2). Vibro-polariton spectra computed by this method are, as expected, equivalent to those obtained via explicitly incorporating cavity parameters in the electronic structure calculation as was done in Refs. 19 and 29. A direct comparison between results obtained via the direct inclusion of the mean field CBOA terms in the energy functional and the effective field approach is shown in Fig. 2 for the case of a CO_2 molecule coupled to a cavity mode. For each system, we present vibro-polariton mode information for a cavity with a photon mode in resonance with the phonon that has the largest IR absorption amplitude. Results are presented for calculations where this resonant cavity mode is the only photon mode included in the calculation (labeled as $N_\alpha = 1, \alpha_{res} = 1$) as well as for the case where seven cavity harmonics are included with the third harmonic being the resonant mode (labeled as $N_\alpha = 7, \alpha_{res} = 3$). Each of these results is presented with and without the inclusion of the adiabatic electronic interaction; plots that artificially neglect this interaction are indicated with the label "$\chi \to 0$."

Results for CO_2 with a cavity mode frequency $\omega_{res} \approx 300\ \text{meV}/\hbar$ in resonant with the A_u vibration mode are shown in Fig. 3. Out of the cases investigated in this work, this system has the closest resemblance to simple models involving a single matter mode "emitter" as the relevant IR active vibration mode is well separated in energy from other degree vibration modes. Indeed, Fig. 3(c) shows results for only a single resonant photon mode with the adiabatic electronic response (χ), which is artificially neglected, yielding the standard Rabi splitting behavior with upper and lower polaritons (LPs) having a similar photon character, IR response, and frequencies, which change essentially linearly with coupling strength (λ) with slopes of opposite sign, but equal magnitude.

In contrast, when the electronic response is incorporated, even the case of a single photon yields asymmetries between upper and lower polaritons, which are seen in Fig. 3(d). This asymmetric energy splitting arises largely from the λ dependence of the $\mathbb{X}$ term in Eq. (30). If we were to decouple the photon mode from the nuclei vibration but not the electronic response, the photonic mode frequency would change as $\omega(\lambda) = \omega(0)/\sqrt{1+\lambda^2\chi}$. Thus, as λ increases, the photon mode is now partially in the "dielectric medium" of the electronic state, leading to a change in frequency, effectively detuning the photon and vibration modes. This results in the nonlinear asymmetric splitting where the upper mode polariton only increases slightly in frequency as in the large λ regime, its character resembles more of a pure vibration mode. Changes in frequency due to hybridization between photon and vibration modes are linear in the coupling strength, while changes

resulting from electronic polarizability go as $1/\sqrt{1+\lambda^2}$, so the lower polariton decreases in frequency at small λ similarly as in the Rabi splitting case, while at large λ, the changes are driven more by the renormalization of the photon frequency by the electronic response. In addition, the inclusion of the electronic response also leads to an additional contribution to the IR amplitude; changes in photon q now lead to changes in matter dipole through the electronic response. The upper polariton mode involves q and ΔR, which favor oppositely oriented dipole moments; thus, the nuclear and electronic changes in dipole moments are in opposite directions, leading to a smaller overall IR amplitude in the upper polariton. The lower polariton, however, involves photon and nuclear displacements, which favor constructive changes in dipole and thus has a larger peak. Furthermore, the electronic change in dipole due to changes in q increases with coupling strength, leading to an increase in the IR absorption of the lower polariton as λ increases. While the ΔR^2 term can also yield asymmetry, this term is included in the $\chi \to 0$ results and is seen to have a much smaller effect compared to the electronic response.

Figures 3(a) and 3(b) show the vibro-polariton spectra when multiple cavity harmonics are included in the calculation. Figure 3(a) shows results in the absence of the adiabatic electronic response ($\chi \to 0$) where there is some mixing of polariton states with initially off-resonant cavity harmonics only at very strong coupling strength. Otherwise, this picture is not so different than the single cavity mode case in the region around the resonant vibration. However, when the electronic response is included [Fig. 3(b)], the spectra are modified in several ways. Since the electronic system responds (adiabatically) to photon displacements, even off-resonant modes acquire an IR absorption strength and have their frequency renormalized as was the case with a single photon mode. Furthermore, once the photon modes are dressed by the electronic response, they are no longer non-interacting even in the absence of interactions with nuclear motion as can be seen in the coupling term between Δq_α and Δq_γ in Eq. (30), which leads to some changes in frequency even between modes that involve no nuclear motion.

These same effects can also be observed in the cases of $Fe(CO)_5$ in Fig. 4, h-BN in Fig. 5, and HfS_2 in Fig. 6, although the spectra of these systems contain a more complicated set of features than CO_2. Differences between how these effects manifest in the vibro-polariton spectra of different systems can largely be understood in terms of each system (free-space) vibrational

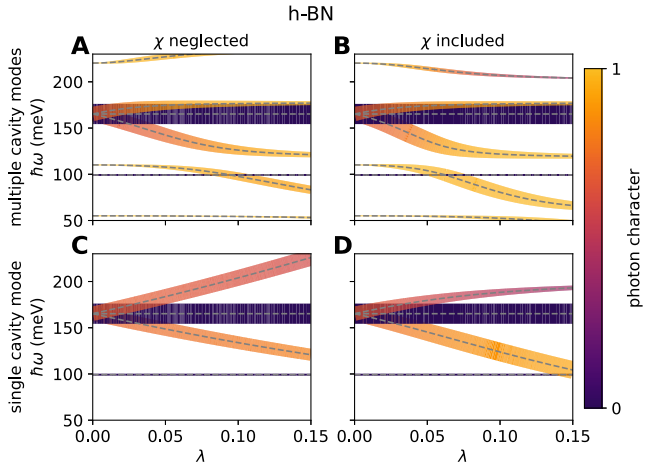

FIG. 5. Computed vibro-polariton spectrum vs coupling strength (λ) for h-BN as a crystalline material. See the caption of Fig. 3 for details on the plot interpretation.

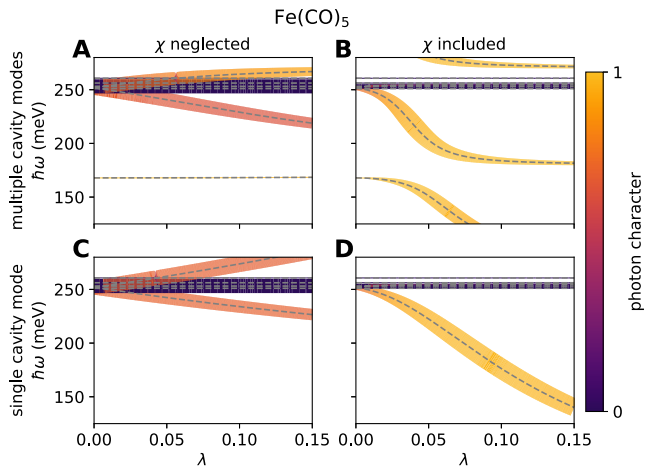

FIG. 4. Computed vibro-polariton spectrum vs coupling strength (λ) for $Fe(CO)_5$. See the caption of Fig. 3 for details on interpreting the plot. The upper right plot contains an inset with the vertical axis scaled to better see the λ dependence in the shown region. As observed here, the electronic polarizability can impact the spectra, IR absorption, and the photon components of the mode eigenvector.

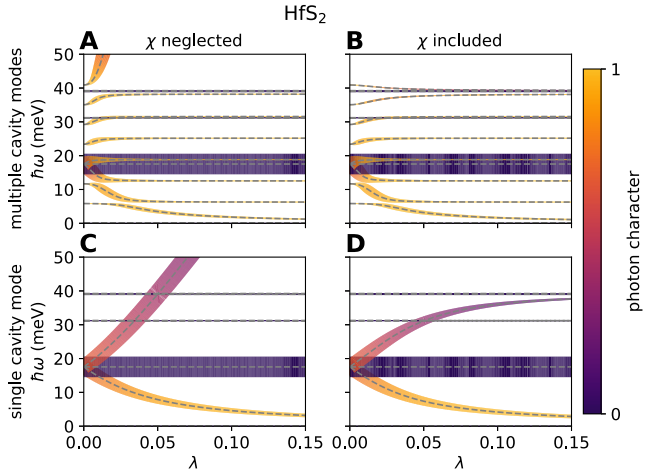

FIG. 6. Computed vibro-polariton spectrum vs coupling strength (λ) for HfS_2. Refer to the caption of Fig. 3 for details regarding the interpretation of the plot. As shown here, the very sharp Rabi splitting of the lowest vibrational mode shown in the plot is moderated in the strong coupling regime by including the electronic polarizability in the calculation of the spectra.

spectra, electric polarizability (χ), and mode effective charges Z^*. These quantities, of which all can be computed with standard (non-QED) density functional perturbation theory, are presented in Table I.

As can be seen in Fig. 4, $Fe(CO)_5$ exhibits a pronounced shift of lower polaritons toward lower energies, as depicted in Fig. 4, when the polarizability is incorporated into the vibro-polariton calculation. This is largely due to the relevant component of the polarizability χ being roughly four times the magnitude as in CO_2. As in CO_2, the dipole moments of the system exhibit constructive changes for ΔR and q in the lower polaritons, while in the upper polaritons (UPs), these changes are destructive. Consequently, incorporating the polarizability χ leads to a reduction in the IR response in the upper polaritons and an enhancement in the lower polaritons. Since χ is larger in $Fe(CO)_5$, this effect sets in more rapidly with respect to increases in λ than in CO_2. The frequency region near resonance in $Fe(CO)_5$ also contains additional IR active modes, although in our model setup, these are not polarized along the same direction as the cavity photon modes do not couple.

Results for the Γ point phonon-polariton spectra of h-BN are presented in Fig. 5. Here, the resonant $\lambda = 0$ IR active modes are twofold degenerate due to the threefold rotational symmetry of the crystal. As we only incorporated cavity photon modes with a single linear polarization direction, the cavity Hamiltonian breaks this symmetry so that at the resonant frequency, one vibrational mode hybridizes with the cavity mode, leading to upper polaritons (UPs) and lower polaritons (LPs), while another purely vibrational "dark" remains at the $\lambda = 0$ frequency. While the inclusion of electronic response χ is observed to lead to an increase in the photon character of the lower polariton with increases in λ, in h-BN, this is seen to occur even when artificially setting χ to zero as can be seen from the lighter color curve of the lower polariton in the bottom left panel of Fig. 5. Aside from the effective detuning of the cavity mode, due to electronic response, this change in mode character as the coupling strength is increased can arise from mixing with other modes of the system, but also from the change in effective vibrational energy due to the ionic DSE. This latter effect becomes more prominent (in terms of percent change of energy level) when the ratio of ionic DSE to the $\lambda = 0$ vibrational frequency is larger. This happens for systems with larger Born effective charges and lower frequency resonant IR vibrational modes.

Results for the Γ point phonon-polariton spectra of HfS_2 are presented in Fig. 6. The underlying physics of this system is similar to that of h-BN, in that a threefold rotational symmetry leads to a similar splitting of the degenerate phonons into UP, LP, and dark modes. However, the differences in $\lambda = 0$ spectra and χ lead to a qualitatively distinct spectra. Compared to the other systems studied in this work, HfS_2 has relevant IR modes with frequencies an order of magnitude lower and dielectric response is 3–10 times larger. The lower initial frequency leads to a larger percentage increase in the upper polariton mode frequency due to the ionic contribution of the DSE, as here this energy is not as small compared to the energy of the relevant vibration modes. In the lower-left panel, where only a single photon mode is incorporated, this effect is seen to lead to a positive curvature increase in upper polariton frequency with λ; however, the inclusion of electronic response χ (right panels) suppresses this feature by changing the λ dependence of the $\Delta R_i \Delta R_j$ coefficient from $\approx \lambda^2$ to $\lambda^2/(1+\chi\lambda^2)$ as can be seen in Eq. (30).

V. CONCLUSION

In conclusion, we have developed an *ab initio* approach for computing the vibro-polaritonic spectra of cavity-coupled matter systems from the matter response to nuclei displacements and applied electric fields. This approach produces results equivalent to previous work implementing a custom cavity Born–Oppenheimer approximation (CBOA) energy functional[19,29] into DFT. In contrast, the method presented in this work uses commonly implemented density-functional perturbation theory results to parameterize the simple harmonic model in Eq. (30) where all cavity parameters appear only in the model. This is achieved by making use of a mapping between the established finite electric field enthalpy functional in DFT calculations[26] and the CBOA energy functional. We illustrate the method with example calculations of the vibro-polaritonic spectra of molecular systems CO_2 and $Fe(CO)_5$ and the 2D solids h-BN and HfS_2. While we use DFPT results to parameterize Eq. (30), we note that the parameters of the matter subsystem (polarizability, Born effective charges, and vibrational modes) can also be accessed by (non-cavity) experiments so that experimental results may be compared to those of the model for the interpretation of polaritonic spectra. Unlike simple two-level models, Eq. (30) can capture asymmetric and nonlinear splitting and other physics. Deviations from the model may then indicate effects beyond the dipole, mean-field, CBO approximations or effects of collective coupling. This relation between electric field response and previous CBOA formulations presented in this work has implications for the understanding of the physics captured in the CBOA, practical implementation of CBOA calculations, and the interpretation of experimental measurements.

ACKNOWLEDGMENTS

We acknowledge funding from NSF via Grant No. EES-2112550 (NSF Phase II CREST Center IDEALS) and startup funding from the City College of New York. All calculations were performed using the computational facilities of the Flatiron Institute. The Flatiron Institute is a division of the Simons Foundation.

AUTHOR DECLARATIONS

Conflict of Interest

The authors have no conflicts to disclose.

Author Contributions

John Bonini: Conceptualization (equal); Data curation (lead); Formal analysis (lead); Funding acquisition (equal); Investigation (lead); Methodology (lead); Project administration (equal); Resources (equal); Software (lead); Supervision (equal); Validation (lead); Visualization (lead); Writing – original draft (lead); Writing – review & editing (lead). **Iman Ahmadabadi**: Formal analysis (supporting); Investigation (supporting); Methodology (supporting); Visualization (supporting); Writing – original draft (supporting); Writing – review & editing (equal). **Johannes Flick**: Conceptualization (equal); Funding acquisition (equal); Investigation (equal); Methodology (equal); Project administration (equal); Resources (equal); Supervision (lead); Writing – review & editing (equal).

DATA AVAILABILITY

The data that support the findings of this study are available from the corresponding author upon reasonable request.

REFERENCES

[1] T. W. Ebbesen, "Hybrid light–matter states in a molecular and material science perspective," Acc. Chem. Res. **49**, 2403–2412 (2016).
[2] F. J. Garcia-Vidal, C. Ciuti, and T. W. Ebbesen, "Manipulating matter by strong coupling to vacuum fields," Science **373**, eabd0336 (2021).
[3] A. Thomas, L. Lethuillier-Karl, K. Nagarajan, R. M. A. Vergauwe, J. George, T. Chervy, A. Shalabney, E. Devaux, C. Genet, J. Moran, and T. W. Ebbesen, "Tilting a ground-state reactivity landscape by vibrational strong coupling," Science **363**, 615–619 (2019).
[4] A. Cygan, A. J. Fleisher, R. Ciurylo, K. A. Gillis, J. T. Hodges, and D. Lisak, "Cavity buildup dispersion spectroscopy," Commun. Phys. **4**, 14 (2021).
[5] J. George, T. Chervy, A. Shalabney, E. Devaux, H. Hiura, C. Genet, and T. W. Ebbesen, "Multiple Rabi splittings under ultrastrong vibrational coupling," Phys. Rev. Lett. **117**, 153601 (2016).
[6] B. Liu, V. M. Menon, and M. Y. Sfeir, "Ultrafast thermal modification of strong coupling in an organic microcavity," APL Photonics **6**, 016103 (2021).
[7] B. Xiang, R. F. Ribeiro, M. Du, L. Chen, Z. Yang, J. Wang, J. Yuen-Zhou, and W. Xiong, "Intermolecular vibrational energy transfer enabled by microcavity strong light–matter coupling," Science **368**, 665–667 (2020).
[8] A. Thomas, E. Devaux, K. Nagarajan, G. Rogez, M. Seidel, F. Richard, C. Genet, M. Drillon, and T. W. Ebbesen, "Large enhancement of ferromagnetism under a collective strong coupling of YBCO nanoparticles," Nano Lett. **21**, 4365–4370 (2021).
[9] G. Jarc, S. Y. Mathengattil, A. Montanaro, F. Giusti, E. M. Rigoni, R. Sergo, F. Fassioli, S. Winnerl, S. Dal Zilio, D. Mihailovic, P. Prelovšek, M. Eckstein, and D. Fausti, "Cavity-mediated thermal control of metal-to-insulator transition in 1T-TaS_2," Nature **622**, 487–492 (2023).
[10] J. Flick, N. Rivera, and P. Narang, "Strong light-matter coupling in quantum chemistry and quantum photonics," Nanophotonics **7**, 1479–1501 (2018).
[11] M. Ruggenthaler, D. Sidler, and A. Rubio, "Understanding polaritonic chemistry from ab initio quantum electrodynamics," Chem. Rev. **123**, 11191–11229 (2023).
[12] J. J. Foley IV, J. F. McTague, and A. E. DePrince III, "*Ab initio* methods for polariton chemistry," Chem. Phys. Rev. **4**, 041301 (2023).
[13] A. Mandal, M. A. D. Taylor, B. M. Weight, E. R. Koessler, X. Li, and P. Huo, "Theoretical advances in polariton chemistry and molecular cavity quantum electrodynamics," Chem. Rev. **123**, 9786–9879 (2023).
[14] J. Flick, M. Ruggenthaler, H. Appel, and A. Rubio, "Atoms and molecules in cavities, from weak to strong coupling in quantum-electrodynamics (QED) chemistry," Proc. Natl. Acad. Sci. U. S. A. **114**, 3026–3034 (2017).
[15] J. Flick, H. Appel, M. Ruggenthaler, and A. Rubio, "Cavity Born–Oppenheimer approximation for correlated electron–nuclear-photon systems," J. Chem. Theory Comput. **13**, 1616–1625 (2017).
[16] J. Galego, C. Climent, F. J. Garcia-Vidal, and J. Feist, "Cavity Casimir-Polder forces and their effects in ground-state chemical reactivity," Phys. Rev. X **9**, 021057 (2019).
[17] J. A. Campos-Gonzalez-Angulo and J. Yuen-Zhou, "Polaritonic normal modes in transition state theory," J. Chem. Phys. **152**, 161101 (2020).
[18] X. Li, A. Mandal, and P. Huo, "Cavity frequency-dependent theory for vibrational polariton chemistry," Nat. Commun. **12**, 1315 (2021).
[19] J. Bonini and J. Flick, "Ab initio linear-response approach to vibro-polaritons in the cavity Born–Oppenheimer approximation," J. Chem. Theory Comput. **18**, 2764–2773 (2022).
[20] M. R. Fiechter and J. O. Richardson, "Understanding the cavity Born–Oppenheimer approximation," J. Chem. Phys. **160**, 184107 (2024).
[21] E. W. Fischer and P. Saalfrank, "Beyond cavity Born–Oppenheimer: On non-adiabatic coupling and effective ground state Hamiltonians in vibro-polaritonic chemistry," J. Chem. Theory Comput. **19**, 7215–7229 (2023).
[22] T. Schnappinger and M. Kowalewski, "Ab initio vibro-polaritonic spectra in strongly coupled cavity-molecule systems," J. Chem. Theory Comput. **19**, 9278–9289 (2023).
[23] T. Schnappinger, D. Sidler, M. Ruggenthaler, A. Rubio, and M. Kowalewski, "Cavity Born–Oppenheimer Hartree–Fock ansatz: Light–matter properties of strongly coupled molecular ensembles," J. Phys. Chem. Lett. **14**, 8024–8033 (2023).
[24] D. Sidler, T. Schnappinger, A. Obzhirov, M. Ruggenthaler, M. Kowalewski, and A. Rubio, "Unraveling a cavity-induced molecular polarization mechanism from collective vibrational strong coupling," J. Phys. Chem. Lett. **15**, 5208–5214 (2024).
[25] R. D. King-Smith and D. Vanderbilt, "Theory of polarization of crystalline solids," Phys. Rev. B **47**, 1651–1654 (1993).
[26] I. Souza, J. Íñiguez, and D. Vanderbilt, "First-principles approach to insulators in finite electric fields," Phys. Rev. Lett. **89**, 117602 (2002).
[27] C. Schäfer, M. Ruggenthaler, V. Rokaj, and A. Rubio, "Relevance of the quadratic diamagnetic and self-polarization terms in cavity quantum electrodynamics," ACS Photonics **7**, 975–990 (2020).
[28] In general, the photon and nuclei kinetic energy operators can act on the electronic wave function through the parametric dependence, leading to an effective vector potential on the slow variables as well as additional terms in the scalar potential. Since we will be investigating dynamics near ground states of non-magnetic systems with an electronic gap (E_{gap}), a gauge can be chosen to make the vector potential term vanish. Contributions to the scalar potential are on the order of $\left(\frac{\omega\lambda}{E_{\text{gap}}}\right)^2$, which we neglect as we will be considering vibrational coupling systems with electronic gaps larger than the photon mode frequencies.
[29] J. Flick and P. Narang, "Cavity-correlated electron-nuclear dynamics from first principles," Phys. Rev. Lett. **121**, 113002 (2018).
[30] ψ may represent the charge density or a Kohn–Sham wavefunction; for our purposes, these are just the electronic variables; particular functionals are minimized with respect to and from which we can evaluate dipole moments.
[31] M. Stengel, N. A. Spaldin, and D. Vanderbilt, "Electric displacement as the fundamental variable in electronic-structure calculations," Nat. Phys. **5**, 304–308 (2009).
[32] S. Latini, D. Shin, S. A. Sato, C. Schäfer, U. De Giovannini, H. Hübener, and A. Rubio, "The ferroelectric photo ground state of $SrTiO_3$: Cavity materials engineering," Proc. Natl. Acad. Sci. U. S. A. **118**, e2105618118 (2021).
[33] S. Latini, E. Ronca, U. De Giovannini, H. Hübener, and A. Rubio, "Cavity control of excitons in two-dimensional materials," Nano Lett. **19**, 3473–3479 (2019).
[34] I.-T. Lu, D. Shin, H. Hübener, U. De Giovannini, S. Latini, M. Ruggenthaler, and A. Rubio, "Cavity engineered phonon-mediated superconductivity in MgB_2 from first principles quantum electrodynamics," arXiv 2404.08122 (2024).
[35] Please note that commercial software is identified to specify procedures. Such identification does not imply recommendation by National Institute of Standards and Technology (NIST).
[36] P. E. Blöchl, "Projector augmented-wave method," Phys. Rev. B **50**, 17953–17979 (1994).
[37] G. Kresse and D. Joubert, "From ultrasoft pseudopotentials to the projector augmented-wave method," Phys. Rev. B **59**, 1758–1775 (1999).
[38] G. Kresse and J. Furthmüller, "Efficient iterative schemes for *ab initio* total-energy calculations using a plane-wave basis set," Phys. Rev. B **54**, 11169–11186 (1996).
[39] G. Kresse and J. Hafner, "*Ab initio* molecular dynamics for liquid metals," Phys. Rev. B **47**, 558–561 (1993).
[40] J. P. Perdew and A. Zunger, "Self-interaction correction to density-functional approximations for many-electron systems," Phys. Rev. B **23**, 5048–5079 (1981).
[41] H. J. Monkhorst and J. D. Pack, "Special points for Brillouin-zone integrations," Phys. Rev. B **13**, 5188–5192 (1976).
[42] N. Tancogne-Dejean, M. J. T. Oliveira, X. Andrade, H. Appel, C. H. Borca, G. Le Breton, F. Buchholz, A. Castro, S. Corni, A. A. Correa, U. De Giovannini, A. Delgado, F. G. Eich, J. Flick, G. Gil, A. Gomez, N. Helbig, H. Hübener, R. Jestädt, J. Jornet-Somoza, A. H. Larsen, I. V. Lebedeva, M. Lüders, M. A. L. Marques, S. T. Ohlmann, S. Pipolo, M. Rampp, C. A. Rozzi, D. A. Strubbe, S. A. Sato, C. Schäfer, I. Theophilou, A. Welden, and A. Rubio, "Octopus, a computational framework for exploring light-driven phenomena and quantum dynamics in extended and finite systems," J. Chem. Phys. **152**, 124119 (2020).